1372 RADIATION CONDITIONS AT A CENTRAL EUROPEAN SQUARE IN A HOT SUMMER DAY, A CASE STUDY FROM SZEGED, HUNGARY

Ágnes Takács[1], Csilla V. Gál[2]*, Ágnes Gulyás[1], Márton Kiss[3] and Noémi Kántor[1]
[1] University of Szeged, Szeged, Hungary; [2] Dalarna University, Falun, Sweden; [3] Hungarian Urban Knowledge Center, Budapest, Hungary

1. INTRODUCTION

In the light of continued urbanization and projected rising temperatures, mitigating the impact of extreme heat events in cities is a pressing urban planning issue. Radiation heat load, quantified as mean radiant temperature (T_{mrt}), has been identified as the main source of summer heat stress and studies has shown that T_{mrt} plays a key role in outdoor thermal comfort conditions (Thorsson et al. 2007, Kántor and Unger 2011, Lee et al. 2014). Consequently, an important task of climate-adaptive urban planning is to create appealing outdoor spaces by providing both sufficient solar radiation and adequate shading. Shading by trees, buildings and devices (such as sun shields) can decrease daytime radiation loads on humans, and thus can mitigate thermal stresses experienced in the urban environment (Lin et al. 2010, Gómez et al. 2010, Makaremi et al. 2012, Lee at al. 2013, Abreu-Harbich et al. 2015, Kántor et al. 2016). The small-scale thermal environments of urban places are not only governed by shade trees and other shading objects, but also by the material properties of adjacent surfaces (i.e. of walls and the ground). Within a wider framework to evaluate the influence of various urban features and nature based solutions (NBSs) on the radiative environment, this study is conducted with a dual aim: (a) to assess the impact of vegetation and different façade orientation on T_{mrt}; and (b) to evaluate the performance of three common numerical models in predicting T_{mrt} values in complex urban environments.

2. MATERIALS AND METHODS

2.1. Study area

The research was conducted in Szeged, Hungary (46.3°N, 20.1°E). The city is the southeastern regional center of the country with an urbanized area of 281 km^2. The city offers an ideal study environment for urban climate and human biometeorological investigations (e.g. Unger 1996, Gulyás et al. 2006, 2009). It is built on a flat terrain with slight topographical differences (78-85 m above sea level), which allows the generalization of the obtained results. Urban land use patters vary across the town—ranging from dense inner city areas to sparse suburban landscapes—and allow for the development of several local climate zone types (Unger et al. 2014).

Szeged has a warm temperate climate with uniform annual distribution of precipitation. The yearly amount of precipitation is low (489 mm), while the number of sunshine hours is high (1978 h). The annual mean temperature is 10.6°C. July and August are the hottest months, and January is the coldest time of the year (Hungarian Meteorological Service – HMS 2015).

Being one of the warmest cities in Hungary, the urban climate of Szeged is expected to be affected more intensely by the rate of warming projected for the Carpathian Basin (Pongrácz et al. 2013). Moreover, Szeged is the third most populated city in the country with more than 162.000 permanent residents. These attributes make the city appealing for urban climate and human biometeorological investigations.

The medium-sized rectangular Bartók square (Figure 1; core area: 110 m x 55 m, plus the surrounding streets) was selected as the study area for the field measurement and for the assessment of small-scale radiation models. The square is located within a 'compact mid-rise' local climate zone in the inner city (Lelovics et al. 2014). It is an important hub of public transit and pedestrians traffic with two bus stops at its opposite sides. The square offers opportunities for recreation and socialization: there is an asphalt-covered basketball–football court at the NW part, several small kiosks on the NE side and benches located across the place. Thus, the place serves the needs of people of all ages. The well-vegetated central and SE parts of the square are characterized by 10–20 m tall deciduous trees (e.g. *Platanus x acerifolia, Tilia cordata, Ulmus procera, Sophora japonica, Fraxinus excelsior, Celtis occidentalis*). Beside the shade from trees, some parts of the square also benefit from the shadowing of the surrounding 3–4 story buildings.

Five measurement locations were selected to investigate the radiation load on pedestrians that either walk on the sidewalks surrounding the square or linger under the mature shade trees in the central area (Figure 2):

- P1, P2, P3 and P4 are located next to SSW-, WNW-, NNE- and ESE-facing facades respectively, ca. 1.3 m from the walls;
- P5 is in the middle of the square, under a 10-meter tall *Sophora japonica* tree with an app. 13-meter wide crown; the station was placed 2 m north from the trunk of the tree.

* *Corresponding author address*: Csilla V. Gál, School of Technology and Business Studies, Dalarna University, 79188 Falun, Sweden; e-mail: cga@du.se

Figure 1: Bartók square of Szeged, illustrated by an aerial image, site photos and an object elevation map

2.2. Field measurements

Two tailor-made human-biometeorological stations were used to record one-minute averages of all atmospheric parameters influencing human thermal comfort (Fig. 3). One of the stations was rotated between the P1–P4 measurement points at 15-minute intervals, while the other remained under the large tree at point P5 for the duration of the entire measurement. Both stations were equipped with a WXT 520 Vaisala weather transmitter to record air temperature (T_a), relative humidity (RH) and wind speed (v). They were also equipped with a rotatable Kipp & Zonen net radiometer to monitor the 3D radiant environment—i.e. to record short-wave and long-wave radiation flux densities from six perpendicular directions (K_i and L_i [W/m^2], i: up, down, east, west, south, north). One of the stations was equipped with CNR 1, and the other with CNR 4 type radiometer. By means of telescopic tripods, the sensors were located 1.1–1.2 m above ground level—at an elevation suitable for human-biometeorological investigations (Mayer et al. 2008).

Typically, in the first position, the arm of the net radiometers was set to face south. In this position, the two pyranometers and two pyrgeometers measured K_i and L_i separately from the upper and from the lower hemisphere (K_u, K_d, L_u, L_d). After three minutes, the net radiometers were rotated manually to the second position where the sensors faced east and west (K_e, K_w, L_e, L_w). After another 3-minute measurement, the arms were turned 90° to measure the radiation fluxes coming south and north (K_s, K_n, L_s, L_n). Considering our 26-hour-long measurement period, this procedure required hundreds of rotations in the case of both stations. Taking into account the response time of the sensors, as well as the time delays due to manual rotation, the first K_i and L_i records following a rotation were removed. Additionally, to record conditions representative of a new thermal environment, the first three-minute data following a relocation were also omitted.

Mean radiant temperature (T_{mrt} [°C]) is a parameter with primary importance in the field of human-biometeorology. It combines all long-wave and short-wave radiant flux densities into a single value in °C dimension. T_{mrt} is defined as the uniform temperature of an imaginary black body-radiating surrounding, which causes the same radiant heat exchange for the human body inside this hypothetical environment as the

complex 3D-radiant environment in the reality (Höppe 1992, Kántor & Unger 2011). T_{mrt} is usually calculated for a standardized standing person. In the case of this study, T_{mrt} was determined based on six K_i and six L_i flux densities obtained from three consecutive positions of the net radiometer:

$$T_{mrt} = \sqrt[4]{\frac{\sum_{i=1}^{6} W_i \times (a_k \times K_i + a_l \times L_i)}{a_l \times \sigma}} - 273.15$$

a_k and a_l are absorption coefficients of the clothed human body in the short- and long-wave radiation domain (assumed to be 0.7 and 0.97, respectively), σ is the Stefan–Boltzmann constant (5.67×10^{-8} W/m^{2}K^4) and W_i is a direction-dependent weighting factor. Assuming standing (or walking) reference subject, W_i is 0.06 for vertical and 0.22 for horizontal directions (Höppe 1992).

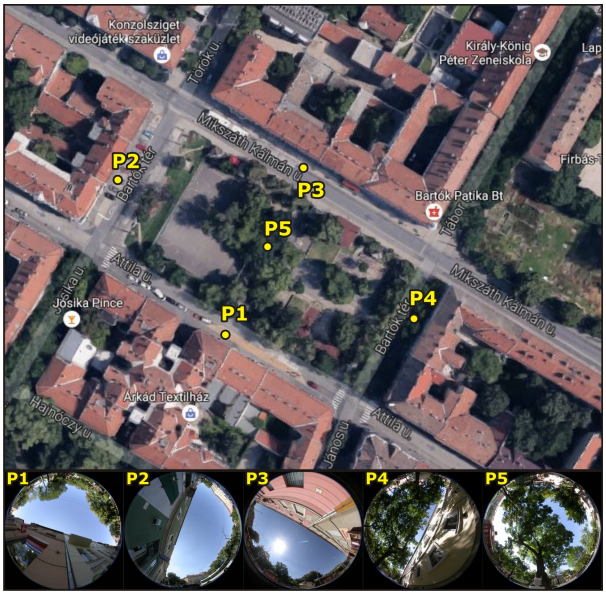

Figure 2: Survey points in the Bartók square with their fish-eye photographs

Figure 3: One of the human-biometeorological stations used in this study (photo taken at P3 location)

The 26-hour-long field campaign spread across two consecutive late-summer days with clear sky conditions (Fig. 4). The measurement period started before sunset on August 7 and ended after sunset on August 8, 2016. According to the data obtained from the nearest urban weather station operated by the Hungarian Meteorological Service (HMS), the temperature ranged from 17.1°C to 26.9°C during the measurement period, and the bell-shaped global radiation curve peaked at 848 W/m2. The clear and calm weather that characterized our measurement period allowed for the development of microclimate differences between the monitored sites to their fullest.

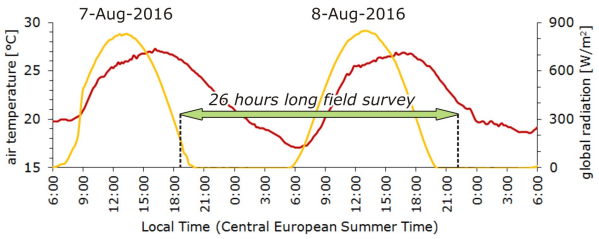

Figure 4: Background weather during the field measurements (10-min average data were obtained from the inner-city weather station of Szeged, 0.9 km away from the survey site)

2.3. Numerical models

Three numerical simulation models were assessed in their ability to reproduce radiative conditions of complex urban environments: ENVI-met (Version 4.0 Preview III), SOLWEIG (Version 2015a beta) and RayMan Pro (Version 3.1 Beta). The study also utilized MATLAB for the analysis of the results.

The digital models of the square were developed utilizing the GIS map of the city, the recent urban tree inventory of Szeged—based on exhaustive field surveys conducted by the Department of Climatology and Landscape Ecology, University of Szeged (Kiss et al. 2015, Takács et al. 2015)—and supplemental onsite and aerial surveys using Google Earth images. As input weather data, all models utilized the 48-hour long (17/08/07–17/08/09) observation from the nearest official weather station operated by the Hungarian Meteorological Service. All numerical simulation models run for the same 48-hour period (starting from 17/08/07) with model states saved at 15-minute intervals. The main numerical-model-specific setups and settings are as follows.

In the case of ENVI-met (Bruse and Fleer 1998, Bruse 2004, Ali-Toudert 2005, Huttner 2012, Simon 2016), the 116x151 size model had a 3-meter horizontal resolution. Besides Bartók square, the model encompassed the eight adjacent urban blocks as well. The vertical resolution utilized the telescopic setup. Thus, the lowest four grids were set to 0.5 meter, while from 2 meter, the height of each consequent grid increased by 20%. The top of the 3D model was at 104,93 m and the tallest building was 38 m. The model trees were adopted from the software's pre-defined,

species-specific, three-dimensional tree catalogue by only adjusting their physical shape and size to match the surveyed values. The materials assigned to the ground surfaces were as follows: gravel asphalt to roads, sandy loam soil to urban blocks and concrete pavement to paved surfaces within Bartok square. The albedo of the gravel asphalt and the concrete surfaces was set to 0.25 and 0.35, respectively. The albedo of roofs and walls was set to 0.35 uniformly. In terms of atmospheric conditions, a simple model forcing was applied with the air temperature and relative humidity values taken from the nearby urban weather station operated by HMS. In order to match the measured maximum global radiation values a solar adjustment factor of 0.98 is applied.

In the case of SOLWEIG (Lindberg et al. 2008, 2011, 2016, Konarska et al. 2014), the Digital Surface Models (DSMs) of buildings and tree canopies were derived from the city's GIS map using 1 meter resolution. The 477x424 digital model encompassed several streets and urban blocks around the square. Based on a long-term shade tree survey in Szeged (Takács et al. 2016a, 2016b), the mean summer transmissivity value of 0.0678—calculated for the most common specie, the Celtis occidentalis—was used in this study. The albedo of walls and ground was set to 0.35 and 0.25, respectively. The input meteorological data was compiled from the above mentioned urban weather station records.

Similarly to SOLWEIG, the files describing the three-dimensional physical environment in RayMan Pro (Matzarakis et al. 2007, 2010) were obtained from the city's GIS map. The procedure requires the 'Shp to Obs' plugin that converts the observation point coordinates, along with building- and tree-related data to the required format. The thus derived five digital models—corresponding to the five measurement locations: P1-5—encompassed the 200m x 200m area surrounding each observation point. Likewise to the other two models, the input weather data were obtained from the nearby urban weather station. For this set of numerical simulations, the 'reduction of G presetting by obstacles' function of the software was turned on.

2.4. Numerical model assessment

The model evaluations were based on the 26-hour-long, 15-minute interval T_{mrt} data calculated from the field measurements and extracted from 48-hour numerical simulation results. The assessment is based on the difference between the model- and the measurement-based T_{mrt} values ($T_{mrt\text{-}mod} - T_{mrt\text{-}calc}$). Besides analyzing differences at each point and comparing model performances over the main study period, we also calculated three parameters recommended by Willmott (1981, 1982): the mean absolute error (MEA), the root mean square error (RMSE) and the index of agreement (d).

3. RESULTS

3.1. Findings of the field measurements

All nighttime air temperatures follow a similar pattern with insignificant differences across the five measurement sites (P1-P5). Differences begin to emerge from sunset, with considerable deviations between the Ta curves developing after 9:00. The period between 12:00 and 13:00 is characterized by the greatest differences, which, in the case of P1 and P3, was around 3°C. In the forenoon, air temperature values of P2 and in the late afternoon, the values of P4 were close to that of P3, which indicate similar radiative conditions at these sites. During the day, air temperatures under the tree (P5) remain relatively low. It should be noted that the more frequent oscillation of the P5 curve is the outcome of its higher data density (with 15-minute interval data recorded continuously), as opposed to the other measurement sites where the 15-minute interval data were collected once every hour.

Similarly to the observed air temperatures, mean radiant temperatures at the five measurement sites followed similar trends at night. However, in contrast to air temperature data, T_{mrt} differences were considerable: at sunset, P3 was over 5°C warmer than P1 and the difference only decreased to 2-3°C by sunrise. During the day, the radiation load differences between the monitored sites increased greatly. In the daytime period till noon, the largest values were recorded at the P2 site. As direct solar radiation became obstructed by the WNW-facing building in the afternoon, Tmrt values decreased. However, because of the long-wave radiations from the heated-up surfaces, P2 remained warmer than the mostly shaded P1 site during most of the afternoon. It should be noted that P1 is located next to SSW-facing facades. Hence, it only receives solar radiation in the forenoon for a rather short period of time. Consequently, the surrounding surfaces are unable to heat up to the extent as the adjacent surfaces of P2 with nearly continuous direct solar radiation exposure.

Among the evaluated sites, P3 (next to the NNE-facing facade) had the most stressful thermal environment with high T_{mrt} values persisting over an extended period of time. This site was exposed to direct solar radiation from late forenoon through sunset, which was accompanied by reflected short wave and emitted long-wave radiations from the gradually-warming surfaces (i.e. road, facade). At this site, radiant temperatures peaked at 75°C and values remained over 70°C between 13:00 and 17:00. Owing to the lack of shade *from trees, buildings or devices* and to the high incoming solar radiation, artificial surfaces adjacent to this site heated up to such an extent that—due to the intensity of their emitted long-wave radiations—this site maintained the highest T_{mrt} values for most of the night.

Among the four measurement sites located next to the facades, T_{mrt} values only leaped briefly at P1 and P4, as they remained essentially shaded though the

day. However, the main difference between them is that in the case of P1 shading was only provided by the SSW-facing façades. In the case of P4, the ESE-facing buildings only shaded the site until 13:00. After a brief period of solar exposure, the site became shaded again by the trees planted along the street. This latter case highlights the role of shade trees in alleviating summertime radiative conditions of urban areas exposed to sun. It is necessary to note that T_{mrt} remained somewhat higher at P4 during dawn because of the presence of shade trees, which similarly to buildings, obstruct the sky and reduce the nighttime radiative cooling potential of a site (P4 had the lowest SVF).

The tall tree at the middle of the square also reduced daytime radiations considerably. The T_{mrt} fluctuations at the P5 site are the results of the crown's heterogeneity that allowed for short-wave radiation to pass through at times. The increases in T_{mrt} values during early-morning and late-afternoon are the outcomes of low sun angles, when direct solar radiation could reach the instrument beneath the large tree crown.

It is also notable that while air temperatures at P3 and P4 were almost identical over the late afternoon, their radiant conditions were almost diametrically opposite: P3 was exposed, while P4 remained shaded by adjacent trees.

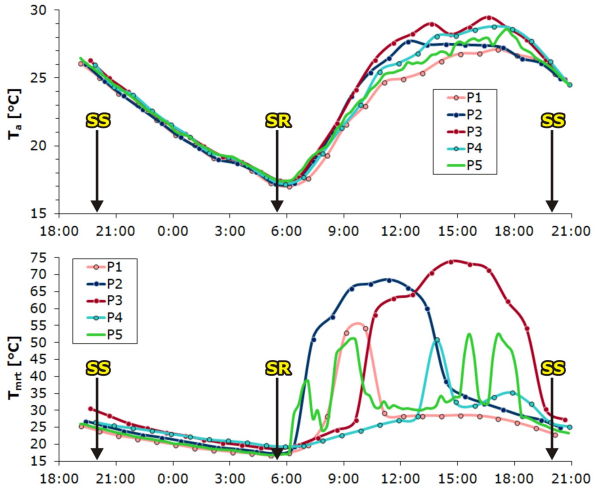

Figure 5: The course of T_a and T_{mrt} at the five observation points (SS: sun set, SR: sun rise; note: data are 15-minute averages)

3.2. Modell validation

It is to be noted to the reader that the results of RayMan have been updated since the poster presentation and thus, the results presented here differ from those in the poster. At the core of the changes were the transition from RayMan (Version 1.2) to RayMan Pro (Version 3.1 Beta).

Figure 6 presents the course of T_{mrt} model errors—expressed as the deviation of modeled values from the measurement-based ones. Model error were calculated for all five observations sites (P1-P5) and for all three numerical models. In general, all models produced similar, location-specific error trends. However, since RayMan Pro frequently under predict daytime T_{mrt} values by about 10°C, SOLWEIG and ENVI-met performed better in emulating the radiative conditions of these complex urban environments.

Similarly to observed T_{mrt} values, model errors were greater during the day then at night. Greater deviation between the errors of different models generally occurred around sunrise and sunset because of differences in digital model resolutions. A good example to this error is the period from around 6:00 to 7:00 in the morning at P1–P3 locations. Here, ENVI-met (the coarsest model with 3m x 3m x 0.5m resolution) lags behind SOLWEIG and RayMan Pro. For the erase of analysis, the time of sunrise (SR) and sunset (SS) are indicated at the bottom of each graph.

The extreme deviations (i.e. peaks and valleys) are the outcome of the mismatch between observed and modeled times when a given observation point becomes irradiated or shaded. A good example for this error is the graph of P2. Here, ENVI-met's error curve dips at 8:00 (indicating that the model still registers the location as shaded), but rebounces by 9:00 in the morning. Similarly, when the observation point becomes shaded in the afternoon at around 14:00, all three models still indicate the presence of direct solar radiation and hence overestimate the actual T_{mrt} values greatly. Nevertheless, this extreme error disappears from the next observation in the following hour. These errors may arise either from coarse model resolutions or from differences between actual and modeled obstructing entities (i.e. trees, buildings or shading devices). For convenience, the periods with direct solar radiation are indicated at the bottom of each graph.

Besides the digital model based errors (due to model inaccuracies and coarse model resolutions), other modeling error trends can also be deduced from the results. First, all numerical models underestimate nighttime T_{mrt} by 5-10°C—except for SOLWEIG, in cases where observation points mostly remain shaded by trees (P4, P5). Second, daytime T_{mrt} in shade is generally overestimated by ENVI-met and SOLWEIG, whereas RayMan Pro hovers near or just below zero (except for P5, which is the result of a subsequently discovered model glitch in which the tree above the observation point was missing its crown). Third, all models underestimate daytime T_{mrt} when observation points became irradiated by the sun.

Among the evaluated models, SOLWEIG's performance is the most consistent with its index of agreement values remaining above 0.80 in all five cases. At the tree-shaded observation sites (P4 and P5)

it achieved the lowest MEA and RMSE values. ENVI-met delivered a comparable performance to SOLWEIG. However, due to its coarse digital model resolution, it slightly underperformed to the firmer. With excluding the problematic P5 result from RayMan Pro's analysis, the results indicate that MEA and RMSE values remain low (around 5°C) in the case of relatively shaded locations (P1, P4) only. In the case of exposed measurement sites (P2, P3), the program underestimates daytime T_{mrt} values by about 20°C on average.

		MAE	RMSE	Index of Agreement
P1	ENVI-met	6.6810	7.6735	0.8867
	SOLWEIG	4.9998	5.9225	0.9250
	RayMan	3.1257	3.8203	0.9567
P2	ENVI-met	8.2693	9.9439	0.9263
	SOLWEIG	6.0269	7.1463	0.9601
	RayMan	8.0931	9.7067	0.9067
P3	ENVI-met	7.8474	8.5602	0.9592
	SOLWEIG	9.5765	12.0570	0.9041
	RayMan	11.6090	14.9120	0.8280
P4	ENVI-met	6.4533	6.9408	0.7995
	SOLWEIG	3.7387	4.8019	0.8412
	RayMan	4.3979	6.2251	0.6740
P5	ENVI-met	6.6660	8.8972	0.8246
	SOLWEIG	4.5759	7.0882	0.8075
	RayMan	8.5765	10.5750	0.7846

Table 1: Summary of the statistical analysis

4. CONCLUSIONS

A complex study comprising of field measurements and numerical simulations was undertaken to investigate radiative conditions and their numerical reproduction at a complex urban environment over a 26-hour long period in Szeged, Hungary. The field data obtained from five measurement points were compared and the performance of three commonly available microclimate models in reproducing Tmrt values was assessed. The field campaign found that daytime radiation loads can reach extreme conditions (Tmrt = 65–75°C) at exposed locations on clear summer days. However, shading from trees can reduce daytime Tmrt highs to 30–35°C. Our filed observations indicate that shading SE-, S- and SW-facing facades and the adjacent sidewalks has the ability to reduce heat stroke cases and to improve human thermal comfort conditions outdoors. The numerical model assessment found that models generally underestimate nighttime Tmrt by 5-10°C—except for SOLWEIG in locations where shade trees were present (P4, P5). Similarly, all three models underestimate daytime radiant conditions when the observation points became exposed to direct solar radiation. In contrast, ENVI-met and SOLWEIG generally overestimates, while RayMen Pro is most accurate in reproducing daytime Tmrt values in shade. Most of the extreme mode errors (peaks and valleys) are the results of digital model inaccuracies and coarse model resolutions.

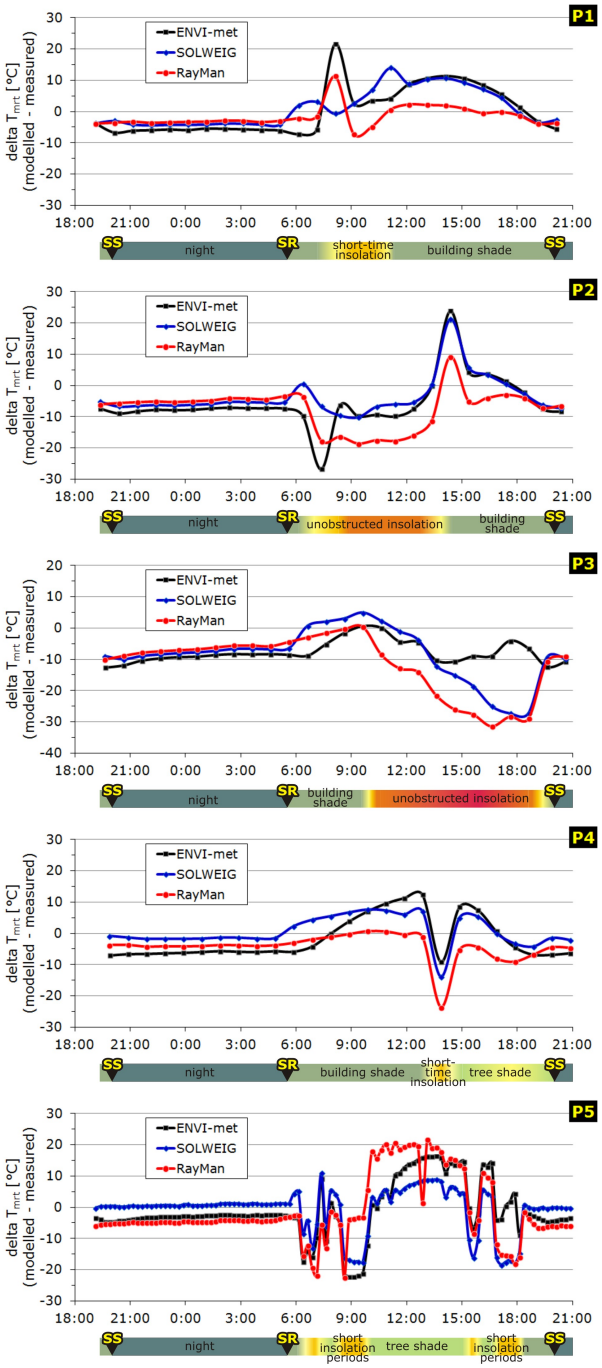

Figure 6: Deviation of the modeled Tmrt values from the measurement-based Tmrt at the five points along the survey period (SS: sun set, SR: sun rise; note: data are calculated from corresponding 15-minute averages)

The recent planning directives of the European Union put greater emphasis on the use of nature-based solutions (NBS) in urban planning. NBSs can not only contribute to re-naturing cities, but are generally more cost-effective than conventional planning approaches. Our field campaign demonstrated that beyond the

commonly upheld benefits of urban trees (such improved air quality, increased biodiversity, contribution to carbon storage and sequestration and decreased cooling needs in tree-shaded buildings), they also decrease heat stresses in cities. With regards to using numerical simulations to access the impact and effectiveness of various NBSs, one has be bear in mind that models always introduce certain degrees of idealization and thus they represent a simplified reality. For example, trees are never as perfectly shaped or have as homogeneous crown transmissivity and leaf area index (LAI) as depicted by digital models, neither are surface parameters as uniform as they are frequently assumed by models. Furthermore, due to the limitations of the numerical models and the many challenges their configuration poses, the ideal outdoor thermal conditions that practitioners often envision for from behind their desks often fail to realize. Thus, identifying the strengths and weaknesses of different numerical models and revealing how they compare to reality is essential for both scientists and urban planners. With proper configuration—aided by model validation and data from field measurements—advance numerical models could become valuable tool to urban green space planning.

ACKNOWLEDGEMENTS

Authors are grateful for the invaluable assistance of Gábor Horváth and Zsuzsa Győri during the 26 hour-long field measurements. The presented study was conducted in conjunction with the Nature4Cities project, which received funding from the European Union's Horizon 2020 research and innovation program under grant agreement No 689817.

REFERENCES

Abreu-Harbich LV, Labaki LC, Matzarakis A (2015): Effect of tree planting design and tree species on human thermal comfort in the tropics. *Landscape and Urban Planning*, 138, 99–109.

Ali-Toudert, Fazia. (2005). *Dependence of outdoor thermal comfort on street design in hot and dry climate*. Universität Freiburg, Freiburg, Germany.

Bruse, M. (2004). *ENVI-met 3.0: updated model overview*. Retrieved from http: //envi-met.net/documents/papers/

Bruse, M. & Fleer, H. (1998). Simulating surface-plant-air interactions inside urban environments with a three dimensional numerical model. *Environmental Software and Modelling*, 13(3–4), 373–384.

Gómez Muñoz VM, Porta Gándara MA, Fernández JL (2010): Effect of tree shades in urban planning in hot-arid climatic regions. *Landscape and Urban Planning*, 94, 149–157.

Gulyás, Á., Matzarakis, A. and Unger, J. (2009): Differences in the thermal bioclimatic conditions on the urban and rural areas in a southern Hungarian city (Szeged). *Berichte des Meteorologischen Institutes der Universität Freiburg*, 18, 229–234.

Gulyás, Á., Unger, J. and Matzarakis, A. (2006) Assessment of the microclimatic and human comfort conditions in a complex urban environment: modelling and measurements. *Building and Environment*, 41, 1713–1722.

Höppe P (1992): Ein neues Verfahren zur Bestimmung der mittleren Strahlungstemperatur in Freien. *Wetter und Leben*, 44, 147–151.

HMS (2015): Climate characteristics of Szeged. http://www.met.hu/eghajlat/magyarorszag_eghajlata/varosok_jellemzoi/Szeged/

Huttner, S. (2012). *Further development and application of the 3D micro-climate simulation ENVI-met*. Johannes Gutenberg-Universität Mainz, Mainz, Germany.

Kántor N, Kovács A, Takács Á (2016): Small-scale human-biometeorological impacts of shading by a large tree. *Open Geosciences*, 8, 231–245.

Kántor N, Unger J (2011): The most problematic variable in the course of human-biometeorological comfort assessment – the mean radiant temperature. *Central European Journal of Geosciences*, 3, 90–100.

Kiss M, Takács Á, Pogácsás R, Gulyás Á (2015): The role of ecosystem services in climate and air quality in urban areas: Evaluating carbon sequestration and air pollution removal by street and park trees in Szeged (Hungary). *Moravian Geographical Reports*, 23, 36–46.

Konarska J, Lindberg F, Larsson A, Thorsson S, Holmer B (2014): Transmissivity of solar radiation through crowns of single urban trees – application for outdoor thermal comfort modelling. *Theoretical and Applied Climatology*, 117, 363–376

Lee H, Holst J, Mayer H (2013): Modification of human-biometeorologically significant radiant flux densities by shading as local method to mitigate heat stress in summer within urban street canyons. *Advances in Meteorology*, 38, 1-13.

Lee H, Mayer H, Schindler D (2014): Importance of 3-D radiant flux densities for outdoor human thermal comfort on clear-sky summer days in Freiburg, Southwest Germany. *Meteorologische Zeitschrift*, 23, 315–330.

Lelovics E, Unger J, Gál T Gál CV (2014): Design of an urban monitoring network based on Local Climate Zone mapping and temperature pattern modeling. *Climate Reserarch*, 60, 51–62.

Lin TP, Matzarakis A, Hwang RL (2010): Shading effect on long-term outdoor thermal comfort. *Building and Environment*, 45, 213–221.

Lindberg F, Grimmond CSB (2011): The influence of vegetation and building morphology on shadow patterns and mean radiant temperatures in urban areas: model development and evaluation. *Theoretical and Applied Climatology*, 105, 311–323

Lindberg F, Holmer B, Thorsson S (2008): SOLWEIG 1.0 – Modelling spatial variations of 3D radiant fluxes and mean radiant temperature in complex urban settings. *International Journal of Biometeorology*, 52, 697–713

Lindberg, F., Onomura, S., & Grimmond, C. S. B. (2016). Influence of ground surface characteristics on the mean radiant temperature in urban areas. *International Journal of Biometeorology, 60,* 9, 1439-1452.

Makaremi N, Salleh E, Jaafar MZ, GhaffarianHoseini A (2012): Thermal comfort conditions of shaded outdoor spaces in hot and humid climate of Malaysia. *Building and Environment*, 48, 7–14.

Matzarakis A, Rutz F, Mayer H (2007): Modelling radiation fluxes in simple and complex environments – application of the RayMan model. *International Journal of Biometeorology*, 51, 323–334

Matzarakis A, Rutz F, Mayer H (2010): Modelling radiation fluxes in simple and complex environments: basics of the RayMan model. *International Journal of Biometeorology*, 54, 131–139.

Mayer, H., Holst, J., Dostal, P., Imbery, F. and Schindler, D. (2008) Human thermal comfort in summer within an urban street canyon in Central Europe. *Meteorologische Zeitschrift* 17, 241–250.

Pongrácz, R., Bartholy, J. and Bartha, E.B. (2013) Analysis of projected changes in the occurrence of heat waves in Hungary. *Advances in Geosciences*, 35, 115–122.

Simon, H. (2016). Modeling urban microclimate: Development, implementation and evaluation of new and improved calculation methods for the urban microclimate model ENVI-met. Mainz: Universitätsbibliothek Mainz.

Takács Á, Kiss M, Hof A, Tanács E, Gulyás Á, Kántor N (2016a): Microclimate modification by urban shade trees – an integrated approach to aid ecosystem service based decision-making. *Procedia Environmental Sciences*, 32, 97–109.

Takács Á, Kiss M, Tanács E, Varga L, Gulyás Á (2015): Investigation of tree stands of public spaces in Szeged. *Journal of Environmental Geography,* 8, 33–39.

Takács Á, Kovács A, Kiss M, Gulyás Á, Kántor N (2016b): Study on the transmissivity characteristics of urban trees in Szeged, Hungary. *Hungarian Geographical Bulletin*, 65, 155–167.

Thorsson S, Lindberg F, Holmer B (2007): Different methods for estimating the mean radiant temperature in an outdoor urban setting. *International Journal of Climatology*, 27, 1983–1993.

Unger, J. (1996): Heat island intensity with different meteorological conditions in a medium-sized town: Szeged, Hungary. *Theoretical and Applied Climatology*, 54, 147–151.

Unger, J., Lelovics, E. and Gál, T. (2014) Local Climate Zone mapping using GIS methods in Szeged. *Hungarian Geographical Bulletin*, 63, 29–41.

Willmott, C. J. (1981). On the validation of models. *Physical Geography*, 2 (2), 184– 194.

Willmott, C. J. (1982). Some comments on the evaluation of model performance. *Bulletin of the American Meteorological Society*, 63(11), 1309–1313.